Magnetic Resonance Imaging Study of Solid Rocket Propellants and Liners

L. H. MERWIN,[1] R. A. NISSAN,[1] T. S. STEPHENS,[1] and A. S. WALLNER[2,*]

[1]Chemistry and Materials Branch, Naval Air Warfare Center, Weapons Division, China Lake, CA 93555, and
[2]Department of Chemistry, Missouri Western State College, St. Joseph, MO 64507

SYNOPSIS

Magnetic resonance imaging (MRI) has been used to study solid rocket propellants and liner material. The samples studied were simulants, used mainly for safety reasons, of real systems using ammonium sulfate in place of the energetic materials. The polymeric binder was hydroxy-terminated poly(butadiene) (HTPB) reacted with isopherone diisocyanate. MRI was used to observe variations in intensity in the simulant samples due to differing percentages of solids loading. It also showed the homogeneous intensity obtained for an unfilled sample used for comparison with the 82% filled material. The liner material, HTPB and dimeryl diisocyanate, was imaged despite its relative rigidity observed from its short T_2 value. Samples of poly(alkylene) oxide simulants were imaged, and various bubbles and regions of filler inhomogeneity were observed. These defects were correlated with photomicrographs of the sample. MRI can be used to image real systems of solid rocket components. © 1996 John Wiley & Sons, Inc.

INTRODUCTION

Solid rocket motors, such as those used on the space shuttle, are composed of a rigid case that contains a thin elastomeric liner and a large area of propellant.[1] This propellant grain consists of an elastomeric material that is highly filled with particulate oxidizer. The homogeneity of the propellant grain and the integrity of the grain/liner/case interfaces are crucial criteria from the standpoint of performance and safety. Properties such as burn rate, mechanical properties, and safety are affected by propellant homogeneity. A method of nondestructive evaluation (*NDE*) would have obvious benefits.

The use of magnetic resonance imaging (MRI) as an *NDE* method in materials science has been well documented.[2] It has been used on various materials, including porous ceramics, wood, plants, and elastomers. Many of the elastomer studies involved swelling the material with solvent and imaging the solvent front. Others imaged the elastomer itself, provided the material was relatively flexible.[2] Finally, some groups used MRI to look at solids content and its affect on the elastomer.[2] These were usually carbon-black filled rubber elastomers. It is therefore an obvious choice for evaluation of rocket motor propellants and liners. These materials are composed of an elastomeric (polymer) binder with a high percentage of a solid, highly energetic oxidizing compound. An initial study using MRI to evaluate solid rocket components has been reported.[3] This study further investigates the usefulness of MRI for evaluating solid rocket components.

In particular, we attempted to focus on issues that are of significance to the solid propulsion community and to use samples which, as close as safely possible, represent current and future solid rocket technology. Samples were prepared with hydroxy-terminated poly(butadiene) as the polymeric binder as this material is currently used extensively in solid rocket motors.[1] Poly(alkylene) oxide, a potential next generation binder material, was also evaluated. Samples were prepared to reproduce, as closely as possible, important structural problems with solid rocket motors. Samples were prepared with and without particulate oxidizer simulant. Samples with various amounts of solid filler were also prepared

* To whom correspondence should be addressed.

Journal of Applied Polymer Science, Vol. 62, 341–348 (1996)
© 1996 John Wiley & Sons, Inc. CCC 0021-8995/96/020341-08

and studied using MRI. Samples were produced which contained deliberately included voids, regions of filler inhomogeneity, bubbles, and other flaws. The images of these samples clearly identify such flaws and defects and demonstrate the applicability of MRI to propellant grain and liner evaluation.

EXPERIMENTAL

Simulants were prepared for several reasons. First, simulants are safer to study than the actual explosive materials. The simulants were also prepared to approach loading levels found in actual materials. Also various physical properties were matched with the actual explosive materials. Preparation of the simulants studied was accomplished using the following methods:

Hydroxy-terminated Poly(butadiene) Propellant System

5 wt % of hydroxy-terminated poly(butadiene) (HTPB) rubber was combined with 0.04 wt % dibutyl tin dilaurate. In a separate beaker, 12 wt % dioctyl phthalate was combined with 0.7 wt % isopherone diisocyanate. All sample weighing and initial mixing were done in a nitrogen atmosphere due to the air sensitive nature of the materials. The materials were then combined and degassed under vacuum for 15 min. 82 wt % ammonium sulfate was added as a simulant for the oxidizer (ammonium perchlorate). The ammonium sulfate used was composed of 56 wt % 200 μm particle size ammonium sulfate and 26 wt % 20 μm particle size ammonium sulfate. Other weight percents were obtained by varying the amount of the smaller particle size ammonium sulfate. The solid simulant was added in small portions and mixed without vacuum until all the solid particles were wet. Additional portions of the solid particles were added in the same manner until the solid was completely mixed. Other samples were prepared with 78 and 80 wt % solids, 0 wt % solids (for comparison), 75.5 wt % ammonium sulfate plus 6.5 wt % aluminum powder, and a sample with 80.5 wt % ammonium sulfate and 1.5 wt % Eccospheres,® which are hollow glass beads that are approximately 20–120 μm in diameter used to simulate voids and bubbles in the simulants (Emerson and Cuming Inc., Gardena, CA). All materials used were reagent grade. Prior to being imaged, each of the HTPB samples was placed in an oven and cured for 5 days under nitrogen at 50°C.

Hydroxy-terminated Poly(butadiene)/Dimeryl Diisocyanate Liner

The liner material was composed of 56 wt % HTPB, 20 wt % dimeryl diisocyanate (DDI), 19 wt % titanium dioxide, 4.7 wt % Cabosil, and 0.3 wt % triethanolamine. This formulation gives an isocyanate/hydroxy (NCO/OH) ratio of 1.4. Other compositions were prepared with varying NCO/OH ratios of 1.0, 0.9, 0.8, 0.7, and 0.6. Each of these variations were prepared separately.

Aluminized Poly(alkylene Oxide) Propellant

The aluminized propellant was prepared with 5.9 wt % poly(alkylene oxide) (PAO), 0.1 wt % hexamethylene diisocyanate, 16 wt % dimethyl phthalate, 13 wt % DE-62 (a mixture of pentabromyldiphenyl oxide, aromatic phosphate, and compatibilizer from Great Lakes Chemical Corporation, West Lafayetter, IN), 15 wt % aluminum, and 50 wt % dechlorane, CAS # 13560-89-9 (Occidental Chemical). Dechlorane was used as an ammonium phosphate simulant since it is compatible with PAO and gives the same density when mixed with the formulation. This material was also mixed under a nitrogen atmosphere. The mixing time was 225 min to allow solids to wet. Initial degassing of PAO was performed for 30 min, and the remaining mixing was done under vacuum due to the air-sensitive nature of the material. The final mixture was then cured for 5 days at 50°C.

Spectroscopic measurements, NMR and MRI, were performed in the following manners:

T_2 Studies

T_2 relaxation times for each material were obtained using a Bruker MSL-200 operating at a proton resonant frequency of 200.130 MHz. The cured solid material was packed in a spinner and inserted into a 7 mm solid-state probe. The data were collected in the static mode. A Carr-Purcell-Meiboom-Gill pulse sequence[4,5] supplied with the Bruker software package was used to collect the data. A variable delay list was used and varied slightly for each material based on the T_2 values expected or observed. The maximum intensity from the data set was picked at each value of the echo time and plotted. The curve-fitting program for relaxation studies supplied with Bruker software was used to calculate the T_2 values by fitting the data to a two-parameter exponential curve. Most data sets were fit to an exponential curve within five iterations. The peak intensity for the

Table I T_2 Relaxation Times for HTPB Propellant Simulant

Filling (wt %)	T_2 (ms)
0	18.73
78	10.95
80	8.67
82	7.84
Eccospheres®	8.97
Aluminum	7.93

CH_2 resonance, which was the most intense peak in the spectrum, was used as a basis for the T_2 calculation. Repetitive runs were performed to ensure reproducibility of the T_2 data.

MRI Experiments

All imaging data were obtained on a Bruker MSL-200 with microimaging accessories. The nucleus of interest was proton, with a resonant frequency of 200.130 MHz. Both conventional spin-echo and multislice pulse sequences were used for data acquisition. The slice thickness in all images was 1 mm. The gradient strengths were 3.013 G/cm in the x- and y-directions and 6.136 G/cm in the z-direction. The z-gradient, combined with a shaped sinc pulse, provided the 1 mm slice excitation. The x- and y-gradients were the read and frequency encode direction, respectively. The image size was 128×128 pixels, taken across a field-of-view of 9 mm. This provided an in-plane resolution of 70×70 μm. The echo time was 5.36 msec for the spin-echo sequence and 5.34 ms for the multislice sequence. The repetition times were 1.0 and 0.5 s for the spin-echo and multislice pulse sequences, respectively. Each experiment was signal-averaged for 48 scans, giving a total acquisition time of 1.7 h for the spin-echo single slice experiment and 0.85 h for the multislice 4-slice experiment.

RESULTS AND DISCUSSION

Before any imaging experiments were run, T_2 values of each material were collected to determine if successful images could be obtained using conventional solution spin-echo pulse sequences. T_2 values were collected for all the HTPB propellant simulant samples with percent filling ranging from 0–82% by weight solid ammonium sulfate. Also, T_2 studies of samples with 1.5% by weight Eccospheres® and a mixture of solids containing 6.5% aluminum powder and 75.5% ammonium sulfate were performed. All these values are contained in Table I.

These results show several things. First, the range of T_2 values for the propellant simulants, being 7.84–18.73 ms, is easily within an acceptable range for MRI studies. Given these values, it is clear that the majority of the signal will rephase during the refocusing portion of the spin-echo sequence and be available for detection.

The second observation apparent from the data is that T_2 decreases with increasing solids loading. This result is intuitively expected. The cured HTPB sample with 0% solids has a longer, almost liquid-like T_2 value. The sample is quite "rubbery," mobile, and fluid-like in its physical appearance. This is supported by its longer T_2 value. As increasing amounts of solid particles are mixed with the binder, the mixture becomes more rigid, and, subsequently, shorter values for T_2 are obtained. This has been observed before with carbon black loading in elastomers.[6-10] In these studies, only a small weight percent of carbon black could be tolerated before the elastomer became too rigid to be imaged in a reasonable amount of time with conventional techniques. This increase in rigidity was due to restricted polymer chain motion. In the HTPB propellant simulant samples, quite high solids loading contents are obtained with reasonably long T_2 values. The materials themselves do become more rigid with the addition of solids. Again, the physical observations are supported by the observed decrease in T_2 values. The T_2 values of the Eccosphere®-filled sample and aluminum-filled sample (both at total solids contents of 82%) are similar to the values obtained for the ammonium sulfate filled simulant.

The T_2 values of the liner material as a function of NCO/OH ratio are given in Table II. As can be seen from the data, T_2 values increase with decreasing NCO/OH ratio. This correlates again with observed physical properties. As the NCO/OH ratio decreases, the liner material becomes more tacky and gummy (i.e., less rigid). This property is re-

Table II T_2 Relaxation Times for HTPB Linear Material

NCO/OH Ratio	T_2 (ms)
1.4	0.612
1.0	1.13
0.9	1.39
0.8	1.76
0.7	2.07
0.6	2.23

flected by an increase in T_2. The range of T_2 values for the liner are near the limits of detection for the pulse sequence used; but with additional signal averaging and/or shorter echo times, it should be possible to obtain an image.

Two MRI images of HTPB propellant simulants are shown in Figure 1. Each image contains an unfilled sample (higher intensity) and a sample with 82 wt % ammonium sulfate (lower intensity). The two images are identical except that the image in Figure 1(b) is at a lower screen contrast than the image in Figure 1(a). Each image shows that solids loading can be differentiated based on intensity. Figure 1(a) shows that the filled and unfilled sample have different levels of signal intensity. The filled sample shows lower intensity due to the high solids loading. The ammonium sulfate does not produce appreciable signal due to its rapid spin-spin relaxation time. The signal generated by the spin-echo pulse sequence disappears quickly (on the order of 100 μsec for solids) before acquisition begins. This short T_2 causes the gray or black portions in the image of the 82 wt % filled sample. Figure 1(b) is at a lower screen contrast to show the homogeneity of the signal in the 0% filled sample. This uniform signal distribution can also be observed in the row profile shown in both figures. The row profile is a projection of the proton density along a particular row or column. The height of the row profile represents the proton density at each voxel across the image. The row profiles clearly show the difference in signal intensity between the filled and unfilled material. The black regions in the filled sample could be due to large ammonium sulfate particles, an agglomeration of several smaller ammonium sulfate particles, bubbles/voids, or some other defect in the sample. This demonstrates the ability to test solid rocket propellant integrity, distinguish different solids loading levels, and detect homogeneity and defects in the propellant formulation using MRI.

To examine the ability of MRI to differentiate solids loading, images of three simulant samples with 78, 80, and 82 wt % solid content were acquired. Figure 2 shows the three samples, appropriately labeled, again at two different levels of contrast, with the corresponding row profile displayed in Figure 2(b). The row profile displayed is marked with a small white arrow at the bottom of the image near the center. This designates the position of the row profile. The display from left to right of the row profile corresponds to top to bottom on the image. As can be seen in the image, the intensity increases from the 82 wt % sample to the 78 wt % sample. The row profile also shows this intensity variation between samples. This is seen both visually and with the row profile. The bright region between the 80 and 82 wt % samples is wax paper used to separate the two samples that were cured together. There is more variation in these row profiles since there is no unfilled material as a reference. Therefore, the

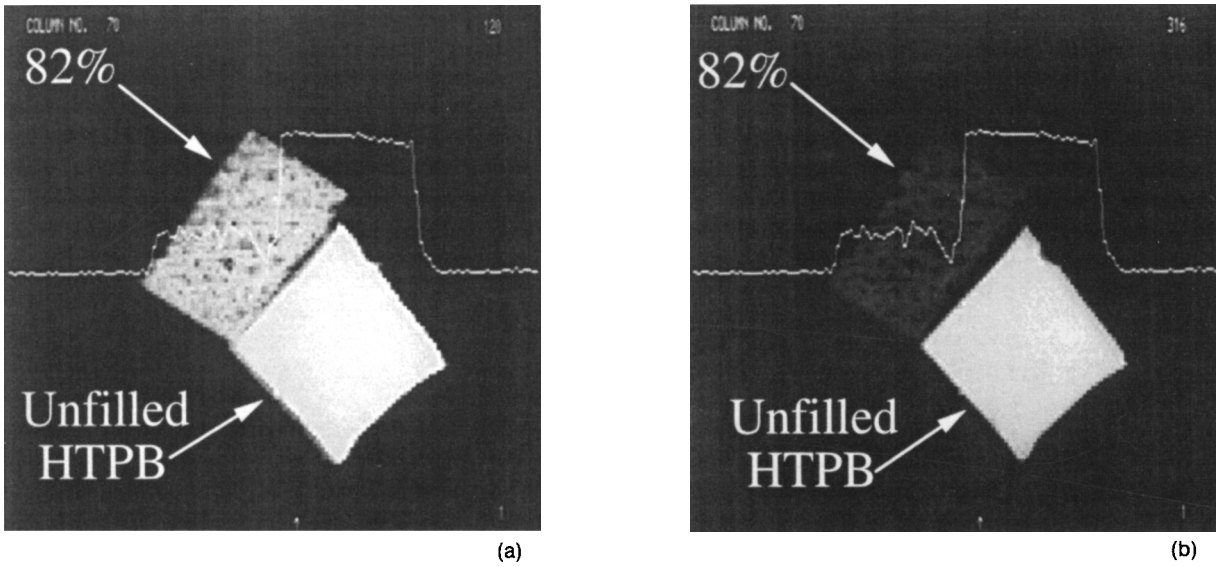

Figure 1 MRI images of 0% (sample on lower right) and 82% (sample on upper left) filled, cured HTPB propellant simulants. (a) High screen contrast and row profile to show intensity differences. (b) Low screen contrast and row profile to show homogeneity of unfilled sample.

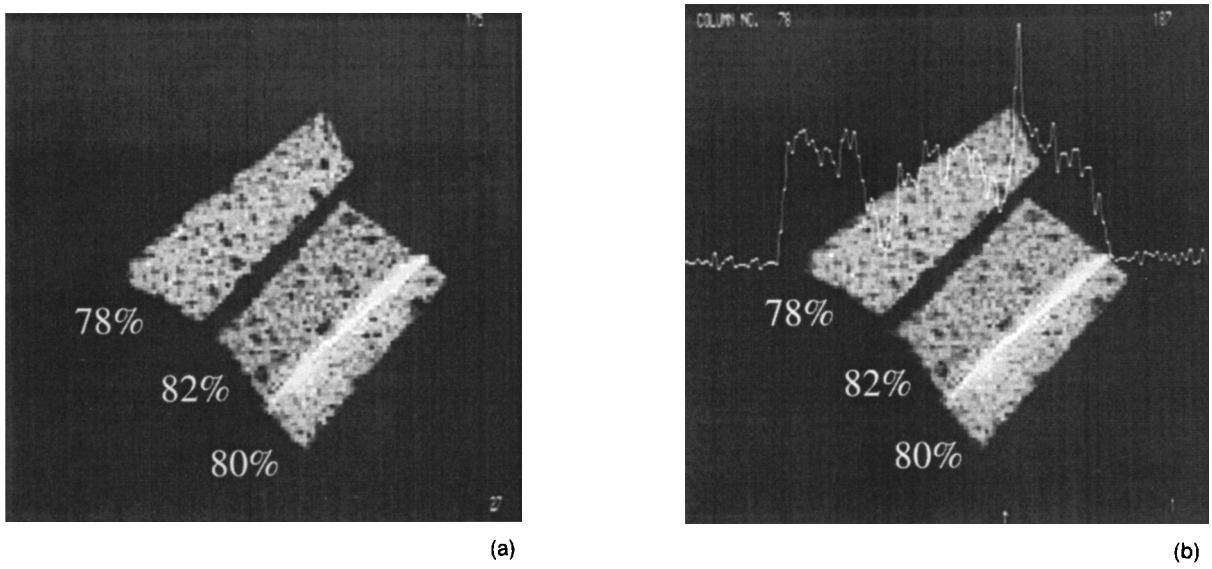

Figure 2 MRI images of HTPB propellant simulants at three different solids loading levels. (a) High screen contrast. (b) Low screen contrast and row profile.

solids loaded materials are the only basis for intensity that the computer screen and instrument have for display. This gives a different scale compared to Figure 1. The scale is a much smaller range of intensity values so noise and variations in the signal are more pronounced. The dark features in the images are again due to either large ammonium sulfate crystals (a large distribution of crystal size was added to the simulant), pockets of several smaller ammonium sulfate crystals packed together, and/or bubbles/voids in the cured material. These images show the ability of MRI to differentiate solids loading levels.

Figure 3 shows a multislice image and an expansion of one slice of an unfilled HTPB sample and a sample filled with aluminum and ammonium sulfate at a total solids content of 82 wt %. Real propellants have a similar weight percent of aluminum added to the formulations. This collection of images was acquired to observe if aluminum had any effect on

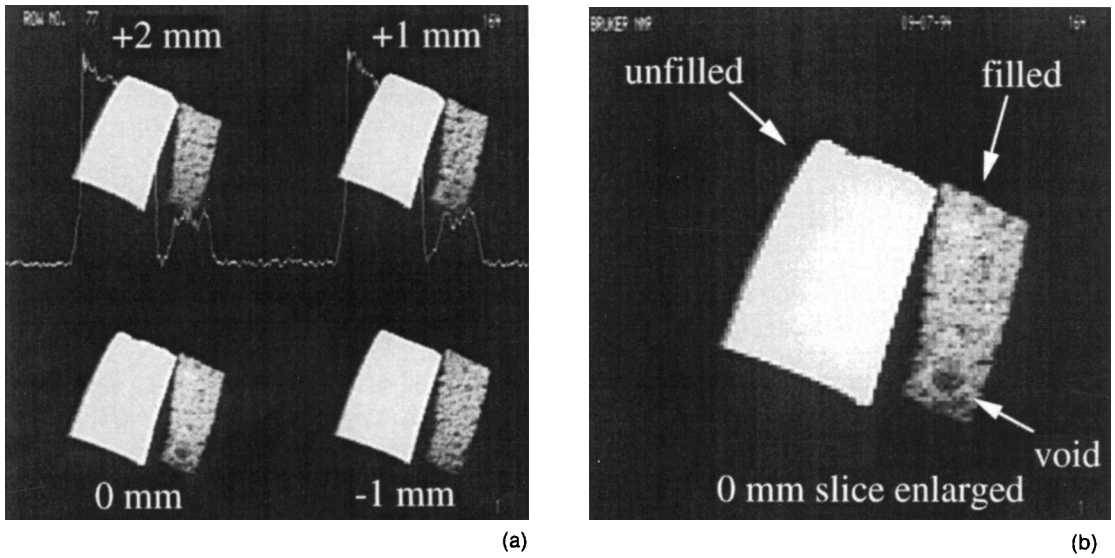

Figure 3 Multislice MRI of unfilled and aluminum-filled HTPB. Aluminum filling at 6.5% with 75.5% ammonium sulfate. (a) Multi-slice acquisition; 4 slices; slice position indicated on figure. (b) Enlargement of 0 mm slice image.

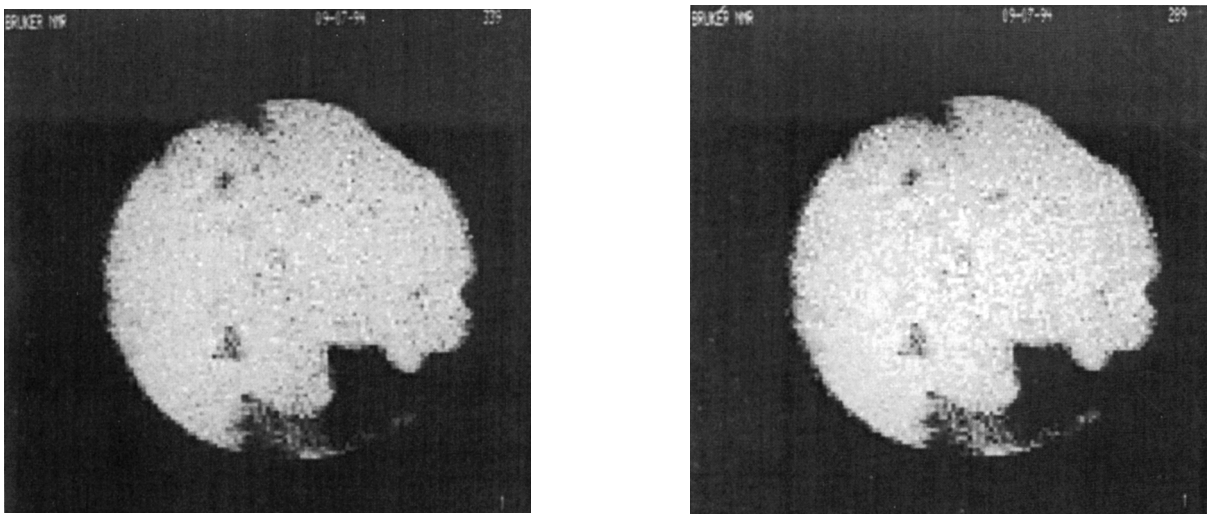

(a) (b)

Figure 4 Spin-echo MRI image of HTPB-based liner material with NCO/OH ratio of 1.0. (a) High screen contrast. (b) Low screen contrast.

image quality due to susceptibility differences. These arise from the large difference in bulk magnetic susceptibility that can exist at an interface between two materials, a metal powder (aluminum) and the hydrocarbon polymer, in this case. Susceptibility interferences are a major difficulty in medical imaging. Others have observed the effect of susceptibility variations on image intensity and quality in materials imaging.[6,7,9-17] Usually an image distortion or a loss in signal is observed at susceptibility interfaces. Susceptibility differences create a local magnetic field gradient across a region of interest. Depending on the difference in magnetic susceptibility and the direction of the read gradient, the particular voxels involved experience a greater or smaller magnetic field than would be experienced with a gradient alone. This difference in applied field creates a mismapping of the affected region and shifts the region along the frequency encode axis. In a spin-echo sequence, a hyperintense region is created from overlapping intensities.[11] These images show no apparent effect on image quality due to the incorporation of aluminum into the sample. The intensity of the image is similar to that of a sample filled with just ammonium sulfate when compared to the unfilled sample (both visually and with the row profile). A void can also be seen in the 0 mm slice position (lower right side).

The liner material is a different material from the binder used in the propellant simulant shown in the first three figures. Although this material is also HTPB-based, it has a much lower solids content and a much higher NCO/OH ratio. Also, the T_2 values discussed earlier are much shorter, showing that this material is more rigid than the propellant simulant (see Tables I and II for comparison of T_2 values). These values of T_2 were at the limit of MRI methods using conventional spin-echo techniques.

Figure 4 shows that the liner material can be imaged successfully with a spin-echo pulse sequence at an echo time of 5.3 ms. The titanium–dioxide-filled liner can be imaged despite its relative rigidity. Several voids and small air bubbles can be seen in the image. The material shown has an NCO/OH ratio of 1.0, although all liners studied gave similar results.

Figure 5 shows a multislice acquisition of a sample of PAO and an expansion of the slice at 0 mm. The images show several regions of low signal intensity due to bubbles and regions of filler inhomogeneity. An estimation of the depth of these defects can be made with the multislice data. The 0 mm slice shows a region of low signal intensity in the center. In the +1 mm slice, the middle portion of this defect is no longer visible. It is also not visible in the −1 mm slice. This defect is limited to a depth of 1 mm. For the lower portion of the defect, it can be seen in the +1 mm slice but is not observed in either the −1 mm or +2 mm slice. This shows that this region of filler inhomogeneity is found to be 2 mm in depth. The bubble located on the left side of the 0 mm slice is also limited to 1 mm in depth as it is not observed in either of the neighboring slices.

The identity of these defects was verified by comparison with photomicrographs of the sample. These photomicrographs are shown in Figures 6 and 7. In

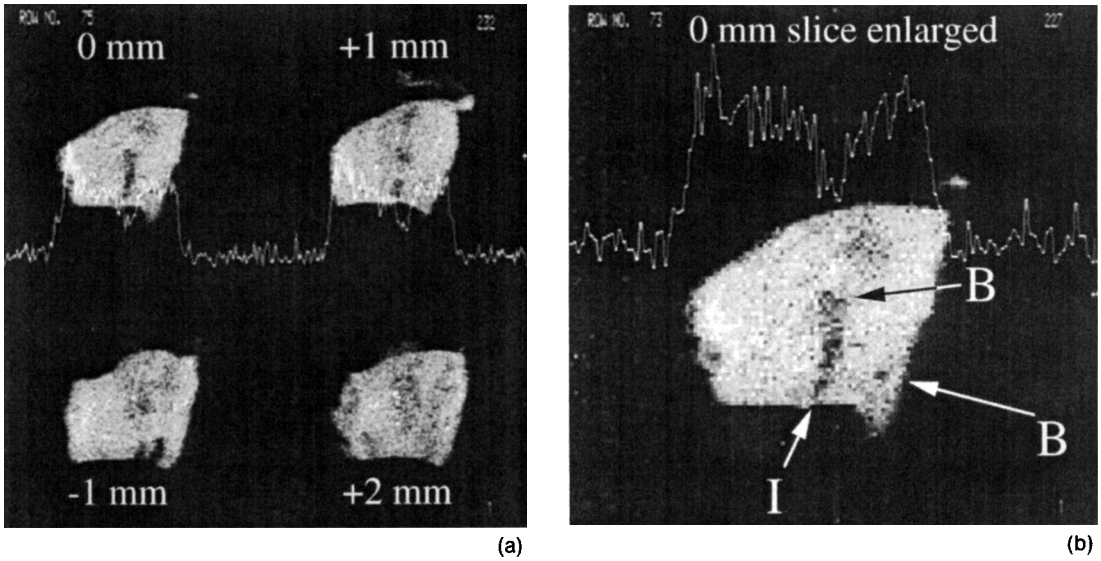

Figure 5 Multislice spin-echo image of filled PAO propellant simulant with 65% solids of which 15% is aluminum. (a) Four slices of sample with slice position indicated. (b) Enlargement of 0 mm slice with defects labeled: B-Bubble, I-Filler inhomogeneity. See Figure 7 for comparison.

Figure 6, the location of the 0 mm slice that was imaged is marked with a dashed line. The bubbles which break the surface in Figure 6 are not seen in the 0, 1, or 2 mm slice in Figure 5(a) but are seen in the −1 mm slice (lower right side of the image). For the second photomicrograph, the sample was cut along the dashed line shown in Figure 6. This cut-away is shown in Figure 7 and represents the 0 mm slice imaged and displayed in Figures 5(a) and (b). As can be seen, the various defects seen in Figure 7 correspond very well with the defects seen in Figures 5(a) and (b). A region of filler inhomogeneity and two regions with bubbles are clearly seen in both the image and the photomicrograph. They correspond well with each other in terms of defect position. This shows the validity of the imaging data and its ability to nondestructively detect defects in these propellant simulants.

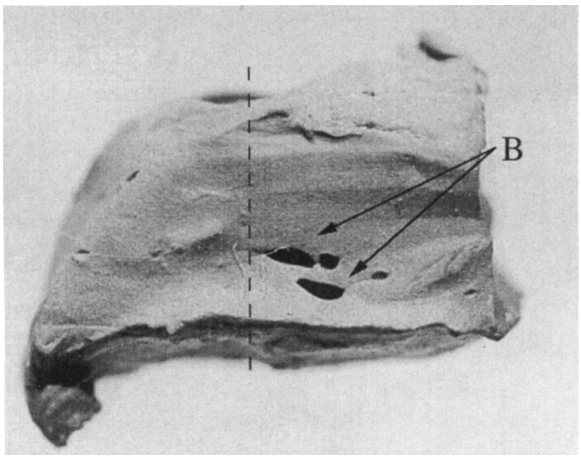

Figure 6 Surface photomicrograph of PAO propellant simulant. The dashed line designates the position of the plane for the 0 mm slice image. B = Bubble.

CONCLUSION

We have demonstrated that MRI can be used as an *NDE* method for real systems of solid rocket components. In the HTPB system, MRI showed an ability to differentiate filled from unfilled samples. From intensity variations, the degree of solids loading was determined relative to other samples in the spectrometer. In addition, MRI provided data on inhomogeneous solids distribution and voids in the HTPB sample matrix. MRI also provided data on the HTPB/DDI liner material showing various voids and defects in the sample. T_2 data for varying NCO/OH ratios in hydroxy-terminated poly(butadiene) suggest that MRI could be used to determine the state of cure of HTPB liners and propellant grains. The use of this technique could have a significant impact on production techniques and quality control.

For the PAO sample, MRI demonstrated the ability to image the material in spite of the presence of embedded aluminum particles. No significant signal loss due to susceptibility variations was ob-

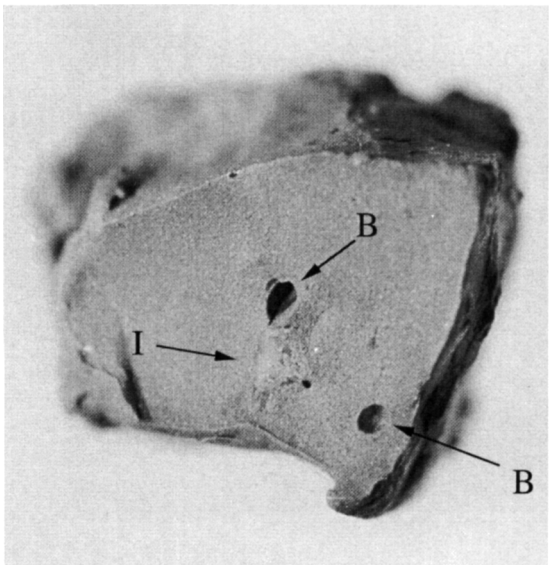

Figure 7 Photomicrograph of the section corresponding to the 0 mm slice of the PAO propellant simulant showing image features. B = Bubble; I = Filler inhomogeneity.

served. Solid-state MRI could be used to determine the kinetics of mobile plasticizer migration from grain to liner and the loss from the grain. This would be a significant tool for aging and service life prediction. MRI also allowed for the visualization of bubbles and inhomogeneous filler distribution in the PAO sample. An excellent correlation between the PAO images and photomicrographs of the sectioned sample show the validity of the imaging data. Future studies include the examination of knit lines and further studies of solids content differentiation. Also, variable temperature work will be used to evaluate sample integrity at various temperatures.

The authors thank Dr. Karen Altmann for proofreading this manuscript. They also thank Dr. Steve Sinton for use of the imaging equipment located at Lockheed Space Center in Palo Alto, CA. We also thank Vicki Brady and Dr. Russ Reed for the PAO samples. Finally, A.S.W. thanks ASEE/ONR for a Summer Faculty Research award that provided funding for him to become involved with this project.

REFERENCES

1. G. P. Sutton, *Rocket Propulsion Elements; An Introduction to the Engineering of Rockets*, 6th ed. Wiley, New York, 1992.
2. W. M. Ritchey, L. Maylish-Kogovsek, and A. S. Wallner, *Appl. Spectrosc. Rev.*, **29,** 233 (1994).
3. S. W. Sinton, J. H. Iwamiya, B. Ewing, and G. P. Drobny, *Spectroscopy*, **6,** 42 (1991).
4. H. Y. Carr and E. M. Purcell, *Phys. Rev.*, **94,** 630 (1954).
5. S. Meiboom and D. Gill, *Rev. Sci. Instrum.*, **29,** 688 (1958).
6. C. Chang and R. A. Komoroski, *Macromolecules*, **22,** 600 (1989).
7. S. N. Sarkar and R. A. Komoroski, *Macromolecules*, **25,** 1420 (1992).
8. L. Garrido, C. C. Sun, J. L. Ackerman, C. Chang, and J. E. Mark, *Polym. Prepr. Am. Chem. Soc. Div. Polym. Chem.*, **31,** 147 (1991).
9. R. D. Kapadia, PhD Thesis, Case Western Reserve University, 1991.
10. L. Maylish-Kogovsek, Ph.D. Thesis, Case Western Reserve University, 1994.
11. S. Posse and W. P. Aue, *J. Magn. Reson.*, **88,** 473 (1990).
12. P. T. J. Callaghan, *J. Magn. Reson.*, **87,** 304 (1990).
13. M. R. Krejsa and J. L. Koenig, *Rubber Chem. Technol.*, **64,** 635 (1991).
14. A. S. Wallner and W. M. Ritchey, *J. Mater. Res.*, **8,** 655 (1993).
15. A. S. Wallner, Ph.D. Thesis, Case Western Reserve University, 1992.
16. K. M. Ludecke, P. Roschmann, and R. Tischler, *Magn. Reson. Imag.*, **3,** 329 (1985).
17. M. S. Cohen and R. M. Weisskoff, *Magn. Reson. Imag.*, **9,** 1 (1991).

Received November 21, 1995
Accepted January 28, 1996